



Relative motion across the eastern Tibetan plateau: Contributions from faulting, internal strain and rotation rates

Zhuqi Zhang^{a,*}, Robert McCaffrey^b, Peizhen Zhang^a

^a State Key Laboratory of Earthquake Dynamics, Institution of Geology, China Earthquake Administration, Dewai Street, Beijing 100029, China

^b Department of Geology, Portland State University, PO Box 751, Portland, OR 97207, USA

ARTICLE INFO

Article history:

Received 26 December 2011
Received in revised form 21 July 2012
Accepted 6 August 2012
Available online 18 August 2012

Keywords:

Block model
Faulting
Internal strain
Rotation
Relative motion
Eastern Tibet

ABSTRACT

A kinematic model comprising 14 rotating, elastic–plastic blocks is used to represent the modern deformation of eastern Tibet and neighboring regions. Block rotations, fault slip rates and permanent strain rates within the blocks are constrained by inverting GPS velocities, slip vector azimuths derived from earthquakes, and fault slip rates derived from geology. The calculated internal strain rates of blocks in eastern Tibet amounts to 10 to 30×10^{-9} /yr, in contrast to relatively low rates ($< 5 \times 10^{-9}$ /yr) in adjacent blocks including the south China, Alxa and Thailand blocks. F-test statistics show that neither the internal strain rates nor the spins of the blocks can be neglected in describing the surface deformation of eastern Tibet. Furthermore, slip on the main faults verifies that the use of deformable blocks can also predict strain localization and strike-parallel variations in slip rates. In terms of east–southeast motion of the eastern Tibetan plateau relative to the Eurasian plate, the net relative velocity contributed by internal strain rates in the blocks amounts to ~ 10 mm/yr, about half of that due to the faulting. In terms of N–S shortening of plateau, however, the internal strain rises to a first order factor west of 95°E , contributing approximately 10 mm/yr, nearly two times larger than that from faulting. The kinematics in eastern Tibet shows that different types of deformation, i.e., NW–SE shear and N–S compression, are taken up by faulting on major faults and distributed contraction, respectively.

© 2012 Elsevier B.V. All rights reserved.

1. Introduction

Among the key questions in the debate on the mechanism of the Tibetan plateau tectonics is whether the deformation is distributed broadly or localized on a few major faults (England and Molnar, 2005; Loveless and Meade, 2011; Molnar and Dayem, 2010; Tapponnier et al., 2001; Thatcher, 2007, 2009). Kinematic analysis may provide clues though large diversity exists in the descriptions of kinematics based on the same data. Analogous to the rigid plate hypothesis for plate tectonics, the principle that the deformation of continents can be represented by interactions among elastic blocks has been successfully applied in some regions (e.g., McCaffrey, 2005; Meade and Hager, 2005). As to the Tibetan plateau, however, although the GPS velocity field has been explained by rotations of a small number of rigid blocks (e.g., Meade, 2007; Thatcher, 2007, 2009), it can also be described by continuum deformation suggesting pervasively distributed strain (e.g., England and Molnar, 2005; Zhang et al., 2004).

In terms of distribution of crustal strain rates, the distinction between the block models and continuous deformation is not entirely

clear. Earlier block models indicated that the internal strain rates in the blocks on the Tibetan plateau are negligible (e.g. Thatcher, 2007). Loveless and Meade (2011) find that small internal strain rates within the Tibetan blocks are needed to fit the residual velocities relative to a rigid block model but they suggest that the internal strain rates are not significantly greater than the level of observational noise. These block models predict fast and uniform slip on major west–east strike-slip faults, indicating strong strain localization. Though continuum models could also allow strain localization along main faults on the plateau, Molnar and Dayem (2010) interpret the localization as concentrations of strain along boundaries of strong medium rather than relative motion between adjacent blocks. These divergent views can be addressed by allowing internal deformation in the blocks and testing whether or not the internal deformation improves the fit to the data and adds significantly to the deformation.

Eastern Tibet undergoes N–S contraction and eastward crustal extrusion relative to the Eurasian plate (Tapponnier et al., 2001). Deformation is composed of zones of strain localization (Molnar and Dayem, 2010) on northeast-to-east-striking strike-slip faults with some amount of strike-parallel variation in rates (Kirby et al., 2007; Zhang et al., 2007) and flow-like crustal motion in the broad area of southeast Tibet (Gan et al., 2007). We use F-test statistics to test the importance of the internal strain rates of eastern Tibet under the framework of block kinematics constrained by multiple types of

* Corresponding author. Tel.: +86 1062009114.

E-mail address: zzqgeorge@gmail.com (Z. Zhang).

data (McCaffrey, 2005). The importance of strain rates is also compared with that of the major faults by estimating how much each contributes to the relative velocities between the eastern Tibetan plateau and the northern margin.

2. Block modeling

2.1. Model settings

In this paper, the surface deformation of eastern Tibet is assumed to consist of a finite number of regions (blocks) whose velocities are due to a combination of internal, horizontal strain rates, rigid rotations on the sphere and interseismic elastic strain accumulation near their bounding faults. The parameters that describe the models are estimated simultaneously by least-squares fitting of geodetic, earthquake and geologic data (McCaffrey, 1996, 2005). The study area includes the extensive plate boundary between India and Eurasia, ranging from Burma–Thailand in the south to Alxa in the north and from the interior of Tibet in the west to South China in the east (Fig. 1a, b and c). Being focused on block kinematics rather than frontal collision, the study avoids the highly deformed Himalayan thrust.

The block boundaries coincide with the major active faults (Deng, 2007) except that the boundary between the north- and south-Qiangtang blocks is inferred from geologic terrane divisions (Pan

and Ding, 2004) and the boundary between the Qingchuan and Qilian blocks is added to separate two distinct patterns of GPS velocities. The strike-slip faults in Tibet (e.g., Tapponnier et al., 2001) are assumed to be steeply dipping. Moderate dips are assigned to the Longmenshan fault and the Minjiang fault, on the east edge of Tibet (Chen et al., 1994; Zhang et al., 2010). Some block boundaries for this region are modified from previous studies (e.g., Meade, 2007; Shen et al., 2005; Thatcher, 2007). Above 10–15 km depth, faults are assumed to be fully locked with a linear transition in locking down to 20–25 km and freely-slipping below 25 km.

2.2. Significance test of model components

The data misfit is calculated in the form of the reduced Chi-square statistic, χ_n^2 , the weighted residual variance divided by the degrees of freedom (DOF = number of data minus number of free parameters). Using more free parameters to match same number of observations in general will result in better fit to the data in the sense of lowering the weighted residual variance but, if the resulting change of χ_n^2 is small due to the increase in DOF, the new parameters may not be deemed necessary to fit the data. By contrast, if the added parameters have great influence on the model fit, the inclusion of those parameters can cause a significant reduction of residuals and subsequently a decrease of χ_n^2 . The confidence that the variance change is not by chance

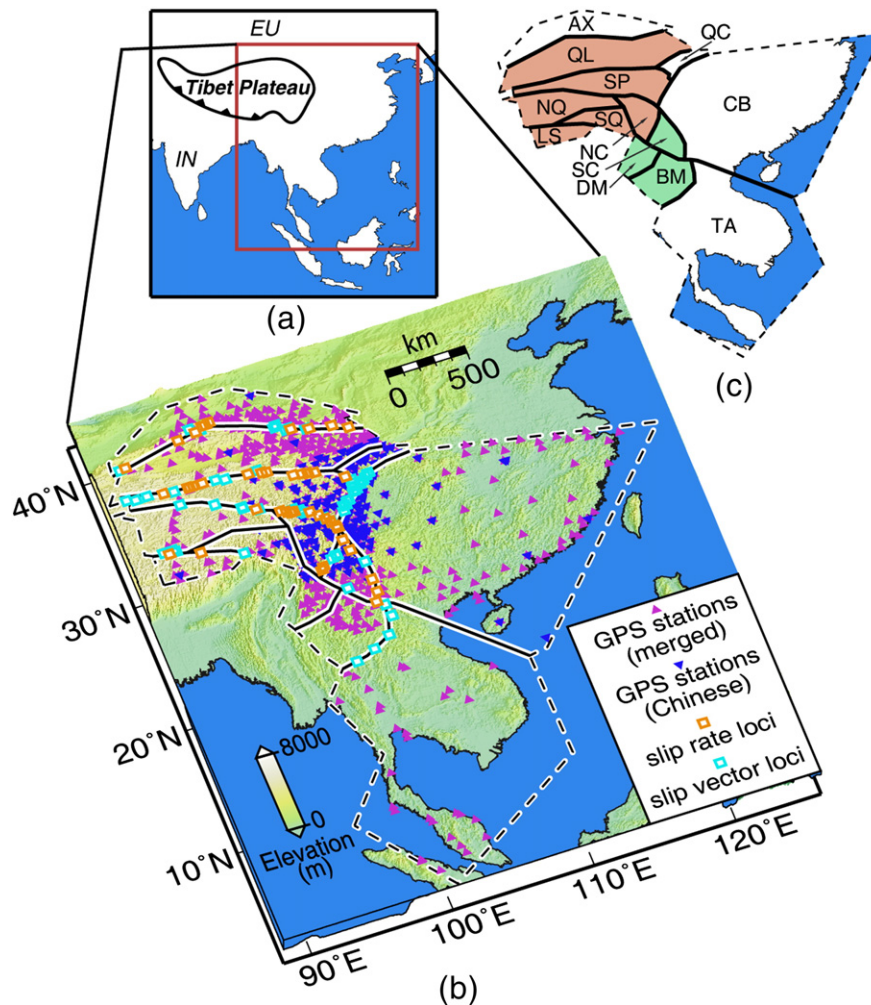


Fig. 1. (a) Study region enclosed by red box. EU and IN are Eurasia plate and India plate, respectively. (b) Map of study region. Solid lines represent block boundaries and dashed line is outer boundary of model domain. (c) Block geometry: block codes are: AX, Alxa; QL, Qilian; SP, Songpan; QC, Qingchuan; NQ, North Qiangtang; SQ, South Qiangtang; LS, Lhasa; NC, North Chuandian; SC, South Chuandian; DM, Dian–Burma; BM, Burma; TA, Thailand; and CB, South China. The blocks on the plateau and those adjacent to the eastern Himalayan syntaxis are highlighted with light red and light green, respectively.

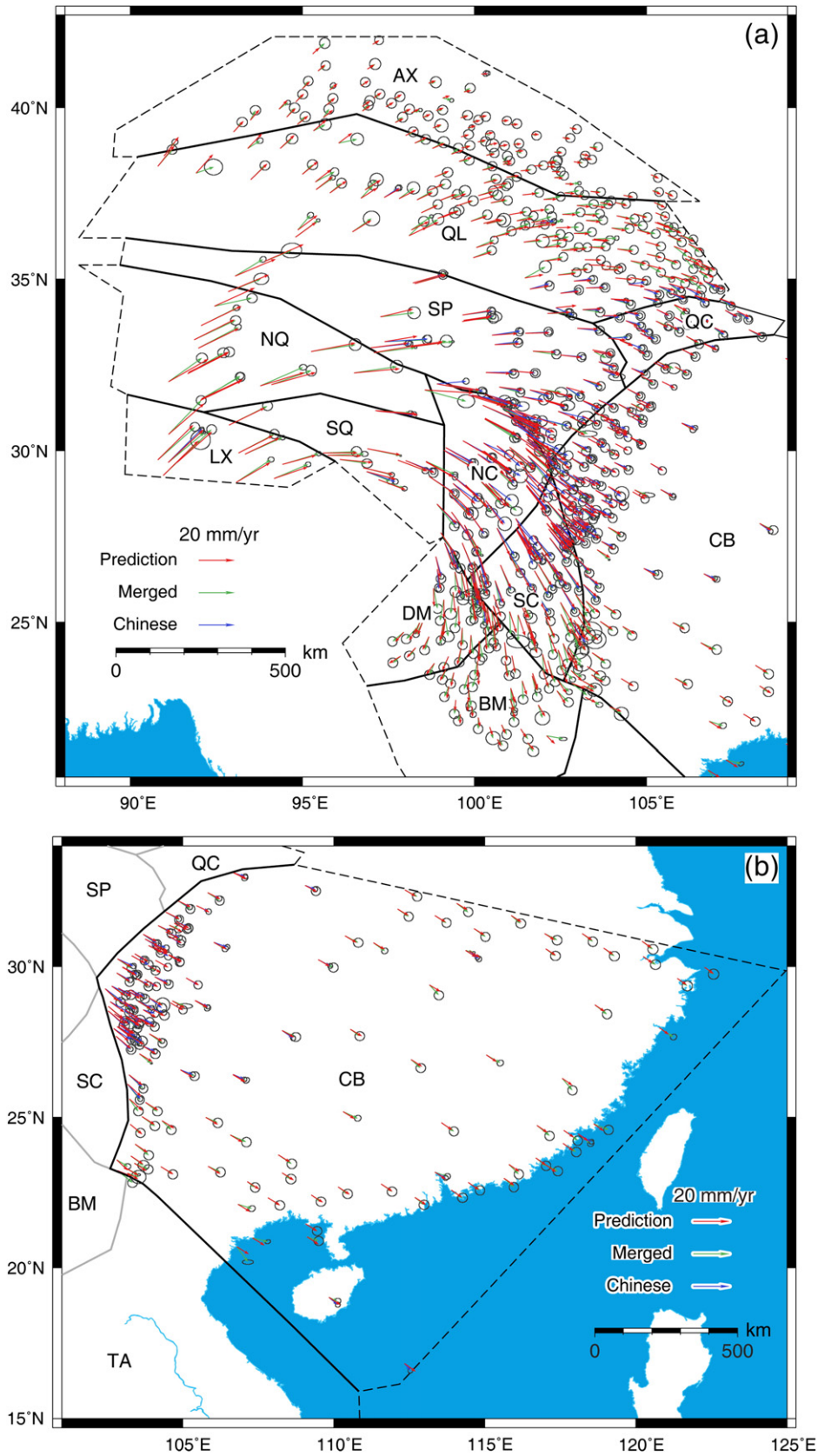


Fig. 2. Observed (green) and predicted (red) GPS velocities with 70% confidence ellipses. Velocities in (a) eastern Tibet, (b) south China (CB) and (c) Thailand (TA) blocks. Solid lines and dashed lines describe the bounding faults and the boundary of the model domain, respectively.

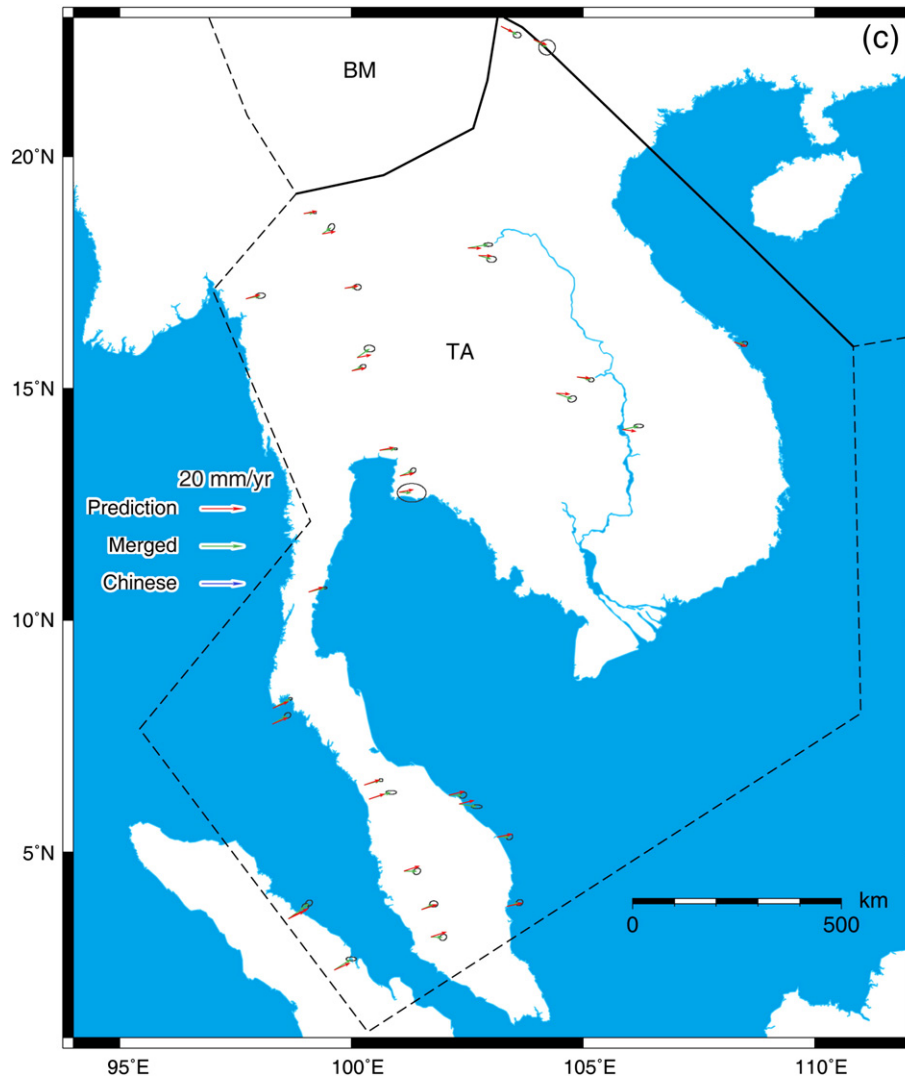


Fig. 2 (continued).

when new parameters are added is evaluated using F-test approach (Stein and Gordon, 1984). A larger variance change for a given change in DOF corresponds to higher confidence that the relevant parameters contribute to the data fit.

In this study, the model attributes surface velocities to solid body rotation, elastic strain along locked boundary faults during interseismic period and optional internal strain rates in the blocks. The significance of the internal strain rate, i.e., the degree to which it is evident in the observed surface deformation, is assessed by the confidence provided by the variance decrease of the model including the strain rate relative to a model without it. Likewise, the significance of vertical axis rotation (spin) of individual blocks is assessed by the variance increase after turning off the spinning of specific block in a model where strain is allowed (a lack of spin in a block means the velocity gradients due to rotation are near zero; equivalent to having a pole of rotation $\sim 90^\circ$ away).

2.3. Data

We use the two horizontal components of 636 GPS velocities from several published studies (Fig. 1b) (Banerjee et al., 2008; Bettinelli et al., 2006; Bock et al., 2003; Calais et al., 2006; Chen et al., 2000; Gan et al., 2007; Jade et al., 2007; Shen et al., 2005; Simons et al.,

2007; Socquet et al., 2006; Sol et al., 2007). The velocities, that we call the merged velocity field, were compiled and rotated into the Eurasian reference frame (Robert W. King, personal communication, 2011). We also use 281 velocities (Supplementary table S1) from the Crustal Movement Observation Network of China (CMONOC) (1997–2009), Sichuan GPS network (2005–2009) and a campaign 973 project (2005–2009). These data, that we refer to as the Chinese velocities, largely overlap the regions of the north- and south-Chuandian blocks and include transects across 3 active faults (Xianshuihe, Anninghe and Xiaojinhe faults). The Chinese velocities are rotated into the Eurasian reference frame during inversion. Velocities with uncertainties of greater than 5 mm/yr and visually obvious outliers in direction or magnitude are removed. The 61 earthquake slip vector azimuths (Fig. 1b) (Supplementary table S2), taken from focal mechanisms (Molnar and Lyon-Caen, 1989; Zheng et al., 2009; Harvard CMT), constrain relative motions along the block-bounding faults. The uncertainties in the slip vector azimuths are estimated with a Monte Carlo method, assuming 10° uncertainty each for strike, dip and rake. The 46 fault slip rates (Fig. 1b) (Supplementary table S3) are collected from geologic studies and their uncertainties are as published (Armijo et al., 1989; Chen, 2006; Gaudemer et al., 1995; Guo et al., 2001; Guo et al., 2007; He et al., 2002; Kirby et al., 2007; Lasserre et al., 2002; Li et al., 2005; Li et al., 2009; Lin and Guo,

2008; Lin et al., 2006; Song et al., 1998; Van der Woerd et al., 2000, 2002; Washburn et al., 2003; Wen et al., 2003; Xu et al., 2003; Xu et al., 2005; Zhang et al., 2007; Zhou et al., 2006).

3. Results

The model parameters are estimated by an iterative, non-linear inversion using downhill simplex (Press et al., 1992) and grid search methods to match the data in a least-squares sense. To avoid falling into local minima, the inversion is accomplished by first fitting GPS velocities without fault locking, which is a linear inversion, then the other data and fault locking are added.

As shown by the map of velocities in eastern Tibet (Fig. 2a), the model with internal strain rates estimated for all blocks predicts velocities with only minor differences from the observations ($\chi^2_n = 1.48$). Small but systematic deviations are found near the east boundary of the Qilian block (QL), an east–west shortening zone (Zhang et al., 1991) not included in our model. The misfit results from modeling simplification and reveals local heterogeneity of internal strain rates. The fit to the velocities in the south China block (CB) is also good (Fig. 2b) except discrepancies at a few sites near the southwest boundary where this block is sliced by several large faults that were active in the Quaternary but activity is uncertain since the late Pleistocene (e.g., Deng, 2007). It is possible that these faults are active at low rates or that the strain rate is a response to the boundary

interaction. The fits to velocities in the Thailand block (TA; Fig. 2c) are relatively poor and the misfits seem to be random, suggesting that the surface deformation in this area may be more complex than uniform block deformation or that the velocities contain postseismic signals from the 2004 earthquake.

The mean uncertainty of the merged velocities (2.4 mm/yr; Fig. 3a) is considerably larger than that of the Chinese data (1.5 mm/yr; Fig. 3b). The Chinese data have lower uncertainties because in general they have longer term observations (supervised under China Earthquake Administration). To test the scaling of the velocity uncertainties, we estimate rotation and internal strain rate in the CB block which appears to deform slowly. Residuals of fits to velocities are random except those in the areas at the west, southwest and east boundaries where local strain may exist (Fig. S2). Hence, only the velocities in the CB block away from the west, southwest, and east boundaries are selected (symbols in red or blue) for analysis. As shown in velocity sections (Fig. S3), the Chinese data exhibit less scattering and a small velocity gradient, compared to the merged data with more scattering and a velocity gradient in the interior of the CB block (Fig. S3a). Following a similar method used by McCaffrey et al. (2007), the cumulative histogram of residual-sigma ratio for the total data set (in the interior of the CB block) is compared with the cumulative Gaussian distribution. The histogram of normalized residuals matches a Gaussian distribution (Fig. S4a). The deficiency shown between cumulative numbers 90 and 100 indicates

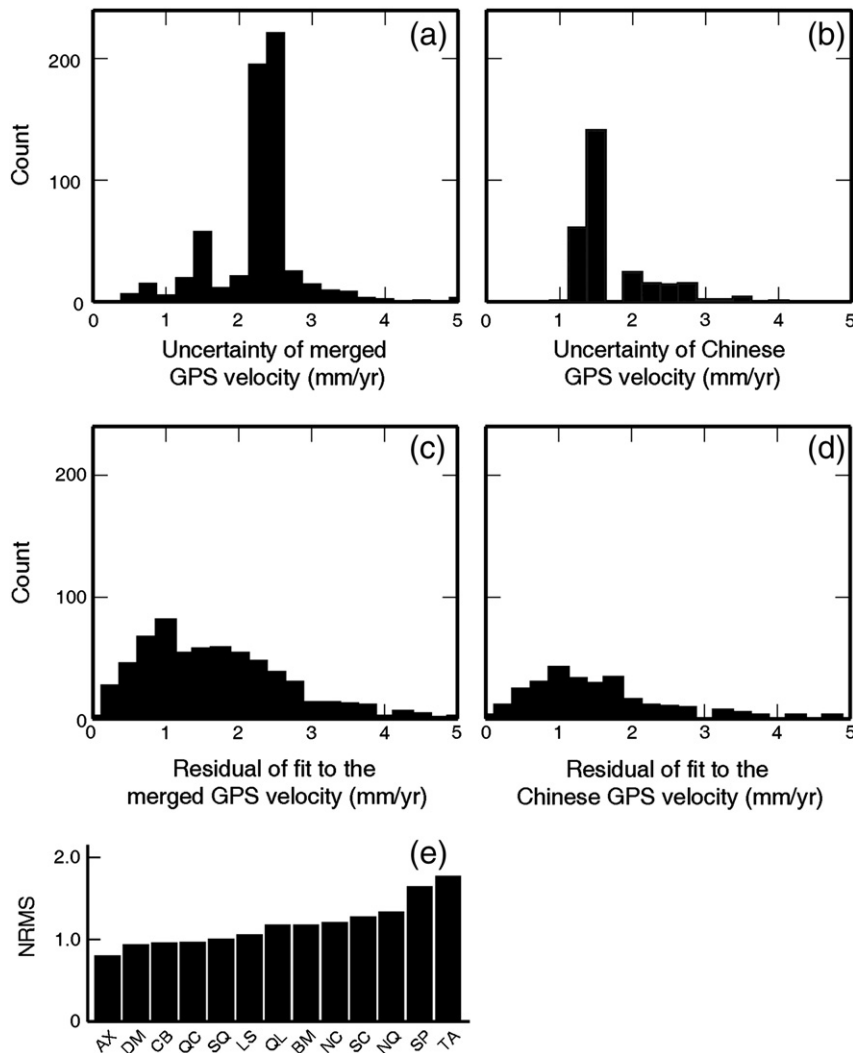


Fig. 3. Distribution of uncertainties of (a) merged and (b) Chinese GPS velocity fields; residuals of the fits to the (c) merged and (d) Chinese GPS velocity fields. (e) Normalized Root-Mean-Square (nrms) GPS misfits by block for model in which all blocks are allowed to deform internally. Block code names are at bottom.

that the distribution of normalized residuals deviates a little with respect to Gaussian distribution. The fits to histograms for individual data sets show that the deficiency exists even for both data sets (Figs. S4b and S4c). The distributions of residuals have similar patterns (Fig. 3c and d), indicating that both GPS fields were fit similarly. The normalized rms (nrms) for the two velocity fields are 1.20 and 1.18, which are both close to 1.0, showing proper weights based on uncertainties. The combination of the relative quality of data, randomness of normalized residuals, and nrms indicates that the uncertainties for two velocity fields have been properly assigned; thus we do not re-scale their uncertainties. The nrms of the fits to GPS velocities within most blocks range from 0.8 to 1.3 (Fig. 3e) indicating that the velocities have been matched at the level of uncertainty in most blocks, except in the Songpan and Thailand blocks where it reaches ~1.5.

3.1. The statistical importance of block deformation

Here, we explore the importance of internal block deformation through statistical tests. The F-test (Fig. 4a) shows that internal strain rates are important for describing the deformation on the Tibetan plateau. The magnitudes of the strain rates (Fig. 4b) for the blocks in eastern Tibet (pink bars) are in general larger than those in adjacent blocks outside the plateau (Calais et al., 2006). Outside eastern Tibet, the Alxa block (AX) and the Thailand block (TA) deform significantly while the south China (CB) and the Qingchuan blocks (QC) are closer to being rigid.

In the north- and south-Qangtang blocks (NQ and SQ), where there are few observations (Fig. 3c), the estimated strain rates are high while the corresponding variance changes are relatively low (Fig. 3b), indicating that the estimation of confidence not only depends on the intrinsic importance of variables but also on the number of observations (Figs. 1b and 4c). By contrast, the lack of internal

strain is properly reflected by low confidence for the south China block CB, that has dense GPS coverage (Fig. 4a and c).

F-tests also show that the spin rates (rotation about vertical axis) of blocks are important for regional deformation (Fig. 4d) on the plateau and around the Eastern Himalayan Syntaxis, except for the Burma block (BM) and Qilian block (QL). Blocks outside the plateau (gray bars) show little rotation.

Apparent strain rates could arise due to existence of systematic velocity discrepancies among different GPS velocity sources. To address this possibility, we run the model using only one published GPS field, that of Gan et al. (2007), which covers most of the study region except the Thailand block. The results show that the strain rates in blocks on the plateau are similar to and somewhat higher than those estimated in the model that used all data (Table S4). In most blocks, the azimuths of maximum contraction from two data sets have differences deviating by less than 13°. In the south China (CB) and Qingchuan (QC) blocks, the deviations are larger than 20°, which may be caused by noise since the significances of strain rates in these two blocks are very low (Fig. 4a). The comparison suggests that the discrepancy among the velocity fields may produce only minor artificial strain. We also assessed the resolution of internal strain rates using a Monte Carlo approach. Similar to the method used by Loveless and Meade (2010), for 1000 trials we added Gaussian random noise of the same uncertainties as the observations to the rotational velocities predicted by the model in which internal strain are allowed for all blocks (Fig. S1). In fitting the 1000 randomly produced fields, to save time, we solved only for the strain rates and rotation poles, which is a linear inversion.

In theory, the predicted strain rates in the tests should be near zero since the trial velocities are due to rotation only. As shown by the distributions of the resulting magnitudes of internal strain rates (Fig. 5), in the blocks SQ, NQ, SP, SC, NC, QL, BM and DM, the simulated strain rates are significantly smaller than the strain

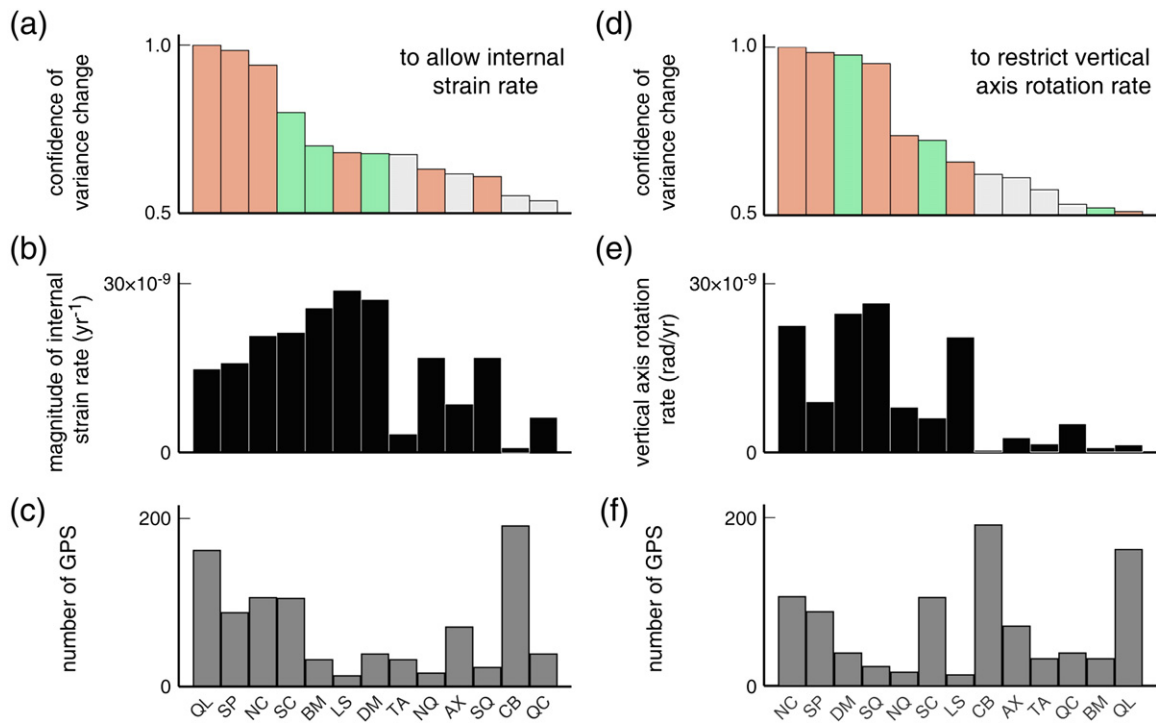


Fig. 4. (a) Confidence of model improvement due to individually allowing strain rates inside blocks; (b) magnitude of internal strain rates; (c) number of GPS sites within each block. Codes at base of (c) identify blocks. A high level of confidence indicates that the block requires internal strain rates to satisfy data. (d) Fit degradation due to imposing restriction on spin rate; (e) vertical axis rotation rates; (f) number of GPS sites. A high level of confidence in (d) indicates that spin rates are required to fit the data. The confidence bars in panels a and d are colored by block as used in Fig. 1c.

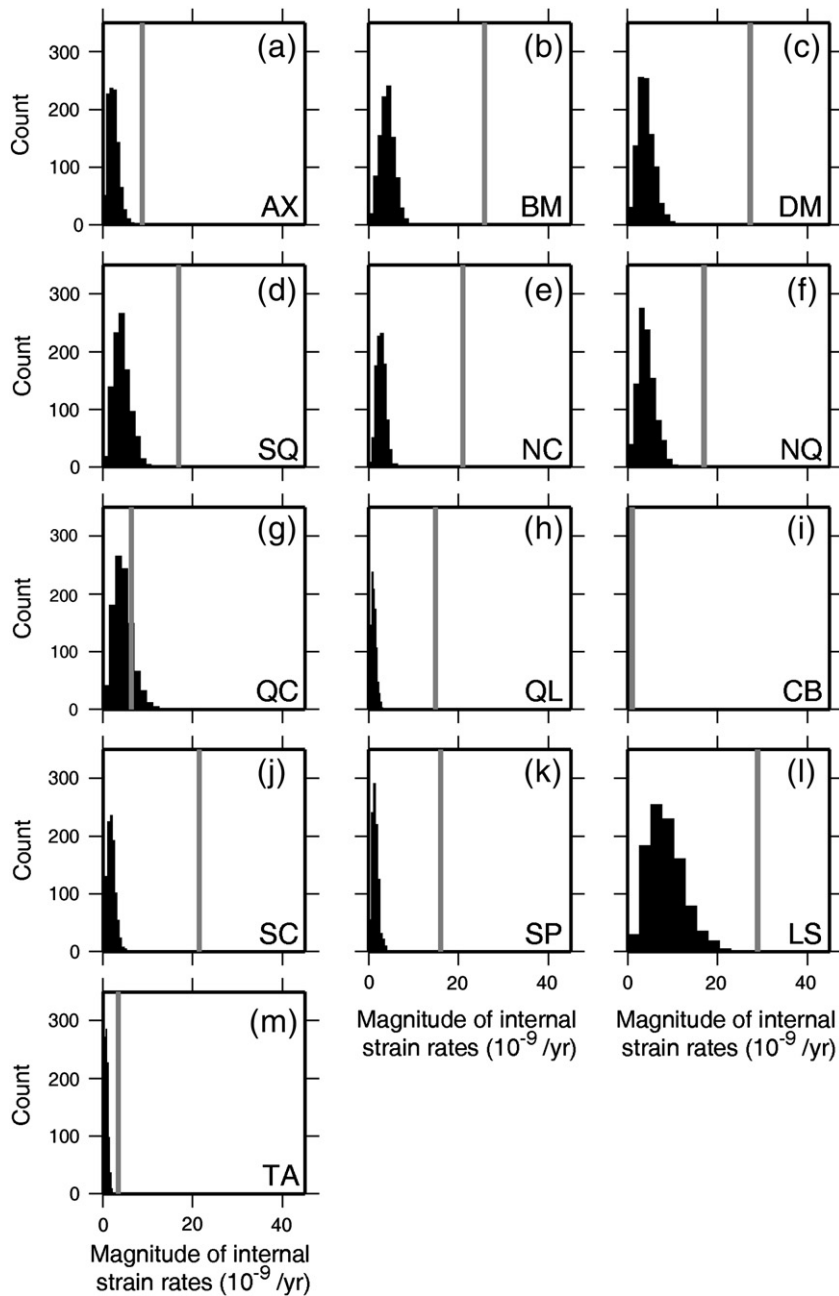


Fig. 5. Distribution of magnitudes of estimated internal strain rates for 1000 Monte Carlo tests. The estimated strain rate (gray line) based on real data is shown for comparison. Block codes are shown at bottom-right.

rates derived from the observations. In the Lhasa block (LS; Fig. 5l), however, while the simulated strain rates are generally smaller than those from the observations they have median value of about $10 \times 10^{-9} \text{ yr}^{-1}$, which is considerably higher than in the other blocks. The LS block is small and has few GPS observations and so the estimated strain rates are more sensitive to noise. In the CB and QC blocks, the simulated strain rates are at a similar level as the observed rates. Hence, the small strain rates in these blocks are not resolvable from zero. In the Alxa block (AX), the simulated strain rates are smaller than the rates from observation, suggesting that though the strain rate in this block is small, it can be detected with the existing GPS network.

The randomness of the simulated strain rates are also evaluated through F-test by comparing the 1000 runs allowing internal strain

rates with corresponding rotation-only inversions. In most blocks, the chances that the improvement is random are generally higher than 30% and concentrate near 50%, revealing the randomness of the simulated strain rates (Fig. 6). The effect of scarce GPS sites is reflected by the different patterns of chance distributions (Fig. 6). Densely covered blocks (e.g., QL, CB, SC, etc.) (Figs. 1b and 4c) have most chances concentrating near 50% while others with fewer GPS sites (e.g., LS, SQ, etc.) have lower probabilities. In other words, with few GPS sites on a block, the possibility that random noise can be mistaken as a strain rate is increased.

According to the results of the above Monte Carlo tests, the estimated strain rates inside most of the blocks on the eastern Tibetan plateau are more likely reflecting true deformation than observational noise.

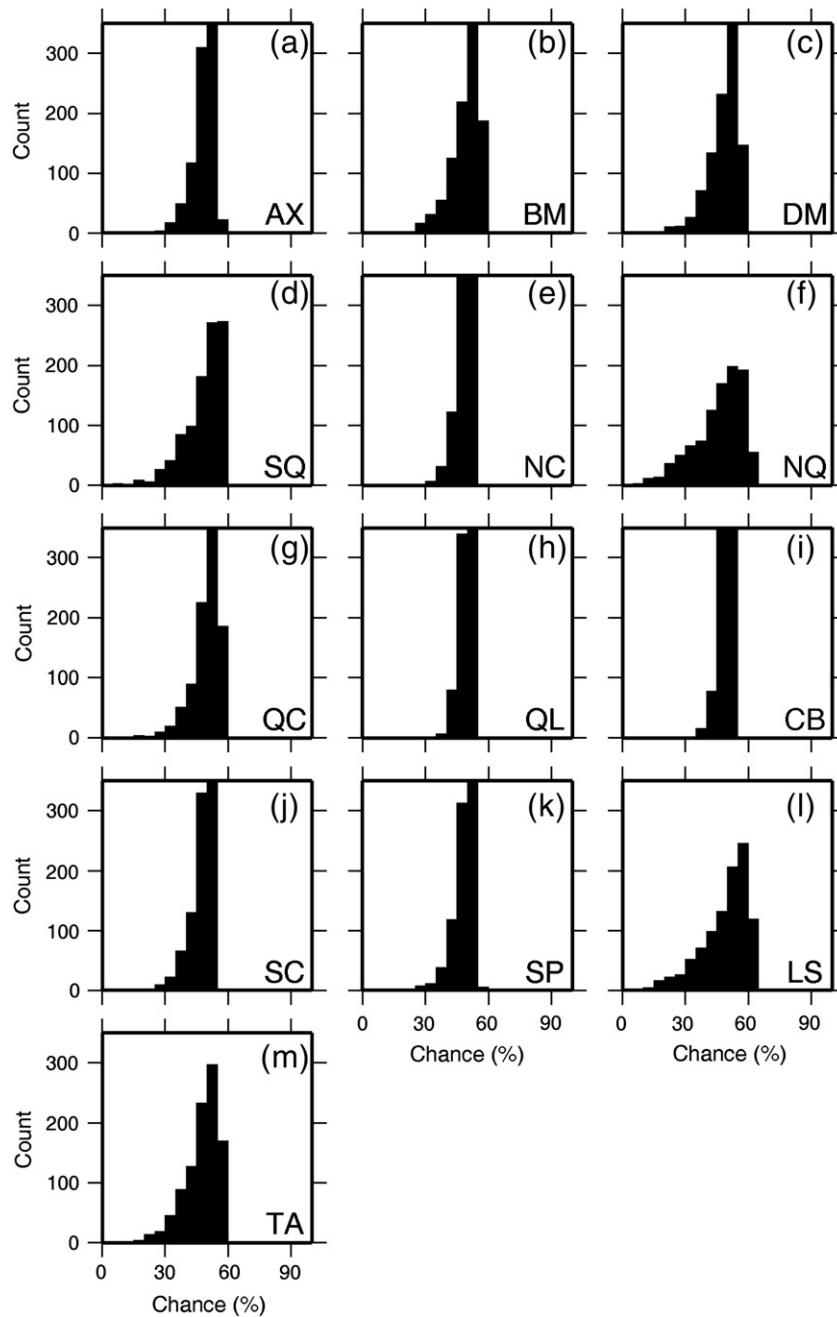


Fig. 6. F-test probability distribution that the variance changes due to allowing internal strain rates are not random in 1000 Monte Carlo tests.

3.2. Fault slip and strain localization on the eastern Tibetan plateau

The model of deformable blocks predicts rapid strike-parallel slip on the faults in and around eastern Tibet (Fig. 7a and b), in agreement with geologic observations (e.g., Tapponnier et al., 2001) and earthquake mechanisms. As shown by the slip rate profiles along the Altyn Tagh and Haiyuan faults (Fig. 7c), the predicted slip rate decrease from about 8 mm/yr at 92°E to 3 mm/yr at 105°E is consistent with the trend of estimates, but at the lower end and showing a great deal of scatter (Li et al., 2009; Zhang et al., 2007). Along the east Kunlun fault (Fig. 5d) the high slip rate on the west segment (Van der Woerd et al., 2000) and low slip rate on the east segment (Li et al., 2005), is considered by Kirby et al. (2007) to be uniform with an abrupt drop at the east end. Lin and Guo (2008) argue instead that, discounting the results of Van der Woerd et al. (2000, 2002) and Li

et al. (2005), the geologic (e.g., Guo et al., 2007; Kirby et al., 2007; Lin and Guo, 2008; Lin et al., 2006) and geodetic (Chen et al., 2000) data reveal that the slip rate decreases continuously from west to east. The trend of slip rate presented in our model shows an eastward decrease (Fig. 7d), in favor of the non-uniform mode.

The predicted slow dextral slip on the western end of the Yushu fault (Fig. 7e) may arise from poor constraints (see Discussion) but there are no geologic observations. On the Jiali fault, the predicted slip rates range from about 5 to 8 mm/yr (Fig. 7f), half of the geological inference of about 15 mm/yr (Armijo et al., 1989). However, a recent study by Chung et al. (2007) found no sign of modern activity on the Jiali fault. The predicted slip of Red-River fault (Fig. 7b and f) is very low (<3 mm/yr), in agreement with early GPS measurements (King et al., 1997; Chen et al., 2000), and this fault was suggested to be inactive in a more recent GPS study by Shen et al. (2005) while Simons et al.

(2007) inferred that the Red-River fault produces dextral slip based on GPS. Rapid slip rates with small variation are found on the Xianshuihe fault (XSH f.; Fig. 7e) and the Anninghe–Xiaojiang fault (AZX f.; Fig. 7g). Left-lateral strike slip at rate of 3–5 mm/yr is found on the Xiaojinhe fault (XJH f.; Fig. 7b and h), which is consistent with the geologic results of Xu et al. (2003). Reverse slip is clear on the

Longmenshan fault (1.5 to 2.0 mm/yr; Fig. 7a and b) and the Minjiang fault (1.5 to 7.2 mm/yr; Fig. 7b and d) at the eastern boundary of plateau.

Assuming the width of the elastic straining zone along these faults is 50–100 km and a slip rate of 1 mm/yr, the elastic strain rates on the faults will be 10 to 20 × 10⁻⁹/yr, which is comparable

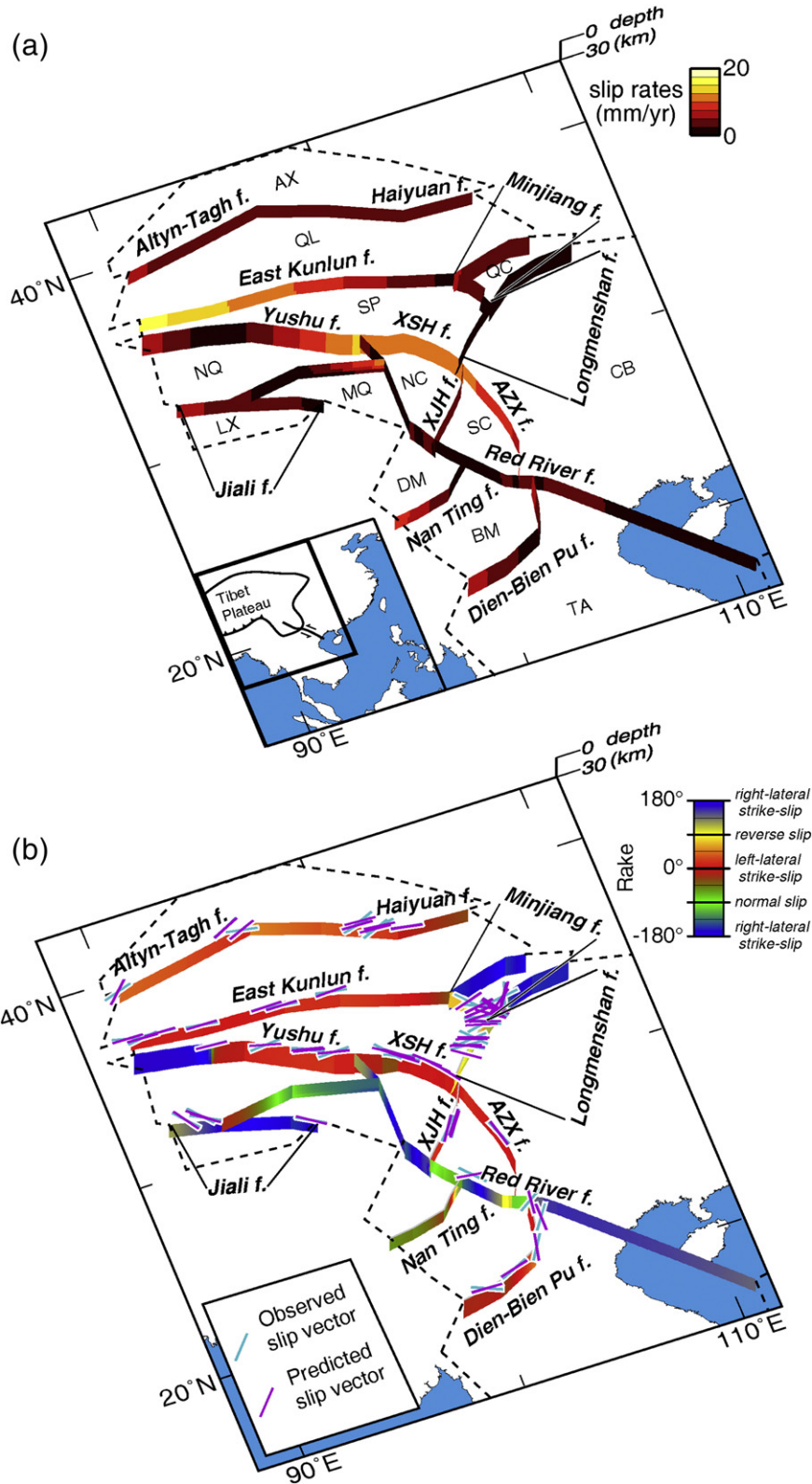


Fig. 7. (a) Predicted slip rates along the major faults; (b) slip vector azimuths and slip sense on faults; and (c)–(h) Black lines show fits to geologic slip rates on the faults with names in (a). Fault codes are: XSH f., Xianshuihe fault; AZX f., Anninghe–Zemuhe fault and Xiaojiang fault; XJH f., Xiaojinhe fault.

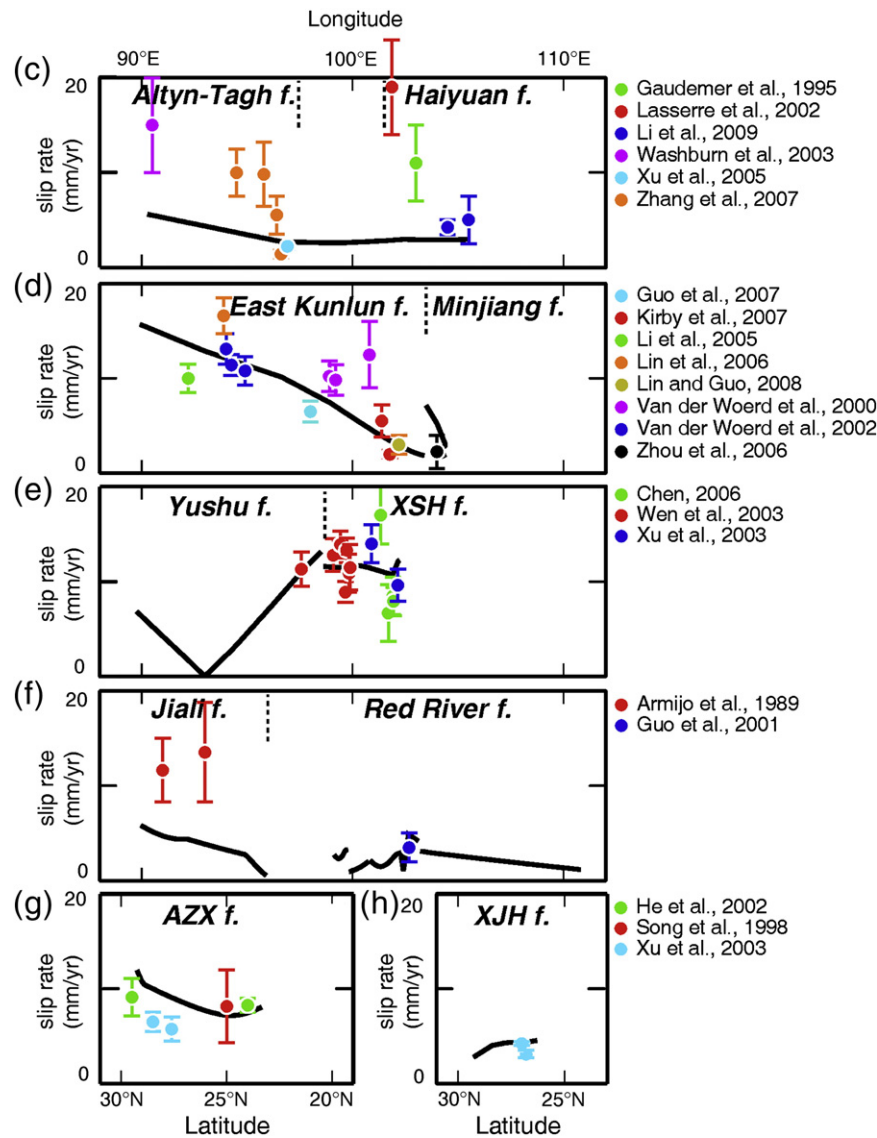


Fig. 7 (continued).

to the strain rate inside the blocks. The prediction of non-negligible slip rates on most faults suggests that strong strain localization occurs on faults on the plateau, and some include along-strike variations in slip rates.

3.3. Relative motion across eastern Tibetan plateau

In eastern Tibet, most blocks have average dimensions of over 300 km, thus the importance of internal strain rates is evident not only in high confidence in F-test but also in contributing to the velocities. The internal strain rates in these blocks amount to 10 to 30×10^{-9} /yr, which is consistent with the levels previously estimated (Calais et al., 2006; Chen et al., 2004; Gan et al., 2007). When multiplied by the block dimensions, the internal strain rate of single block (DM, LS, SQ, NQ, SP, NC) would account for relative velocity at the level of 3 to 6 mm/yr.

The vertical axis rotation rate (VAR) of a block is the dot product of its angular velocity with a unit vector pointing from the center of the Earth to the center of the block at the Earth's surface. One can think of block motion as the combination of the VAR and a 'translation', which is the motion about an axis 90° away from the block but in the plane

of the angular velocity. Hence, the VAR, or the spin rate, describes the gradients of velocity due to the rotation of the block. Therefore, the 10 to 25×10^{-9} rad/yr spin rates of most blocks on the plateau (i.e., NC, SP, DM, SQ, NQ, SC and LS) (Fig. 4e) also contribute significantly to the relative motion.

The comparison of the contributions of rotation rates, internal strain rates and faulting to the total motion of the south plateau relative to north margin is carried out along four velocity profiles in the direction of India–Eurasia convergence (Fig. 8a). The direction of convergence is based on the Euler pole of the India plate in the Eurasian reference frame. The Euler vector estimated by fitting GPS velocities is (26.172°E , 27.626°N , $0.4417^\circ/\text{Ma}$), which yields the convergence azimuths of 16.8° , 17.5° , 18° and 22° for profiles AA', BB', CC', and DD', respectively (Fig. 8a). To reveal the shortening and the lateral extrusion with respect to collision, the velocities are resolved in the direction of the profile (radial component) and normal to it (transverse component) along the profiles. The radial velocity is positive toward the NNE and the transverse velocity is positive toward WNW. Under this sign convention, with the x-axis increasing to the NE, a negative slope in the radial velocity represents shortening (Fig. 8b–i) while a negative gradient in transverse velocity means the northeast end of

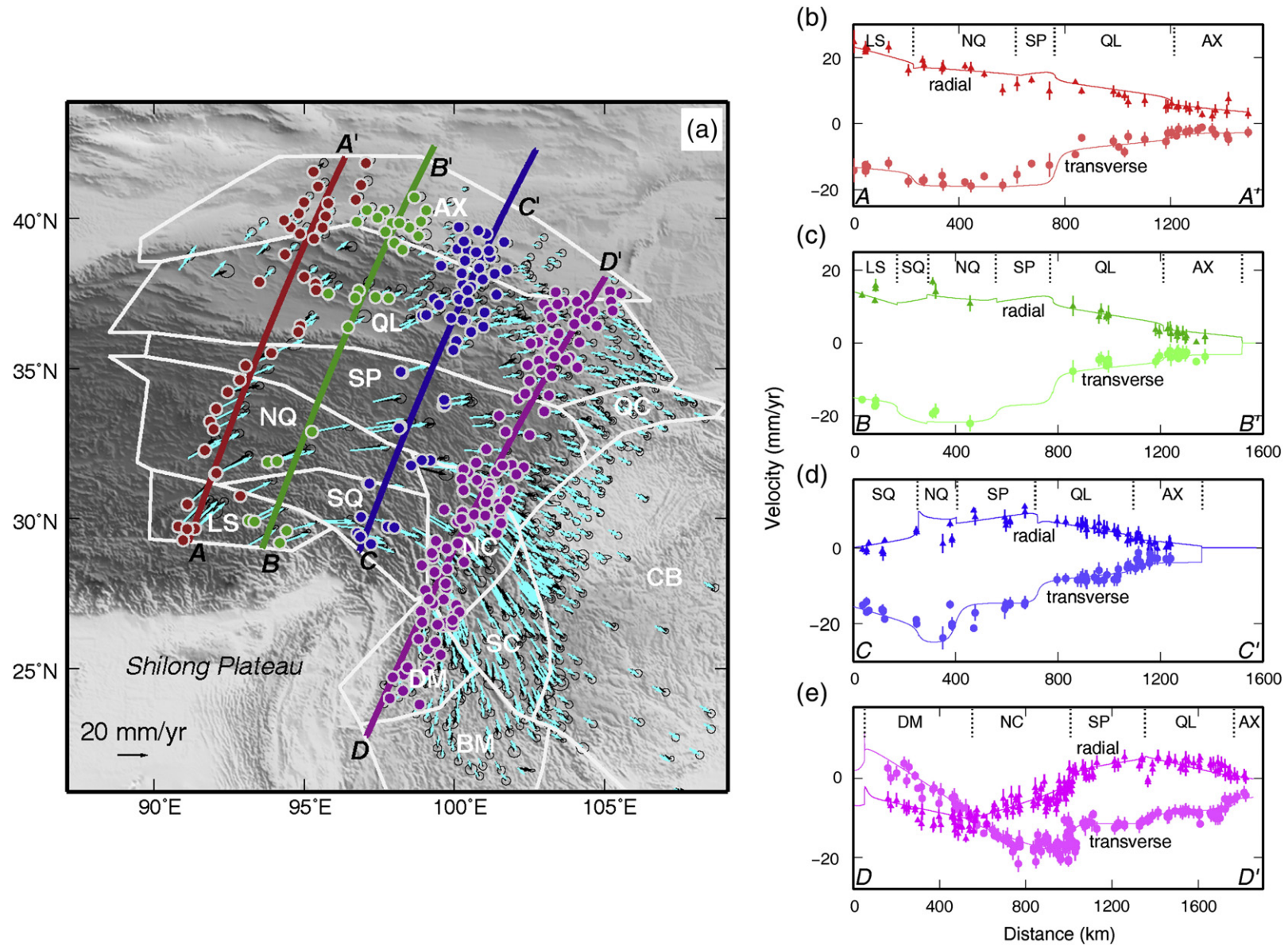


Fig. 8. (a) Locations of velocity profiles used in estimating the velocity budget across the region. Each profile is marked in a unique color. The black and cyan arrows represent the observed GPS and predicted velocities, respectively. Observed GPS sites used in each profile are marked with circles in corresponding colors. White polygons outline the blocks. (b)–(e) Calculated velocity profiles (solid lines) and observed GPS data. The color scheme follows that used in (a); heavier lines for radial component (parallel to profile) and lighter lines for transverse component (normal to profile). Triangles and circles with error bars represent observed data in radial and transverse directions, respectively. (f)–(i) Profiles of radial velocity component due to strain rates (thick lines) and faulting (thin lines). (j)–(m) Profiles of transverse velocity component due to strain rates (thick lines), faulting (thin lines) and vertical axis rotation (dashed lines).

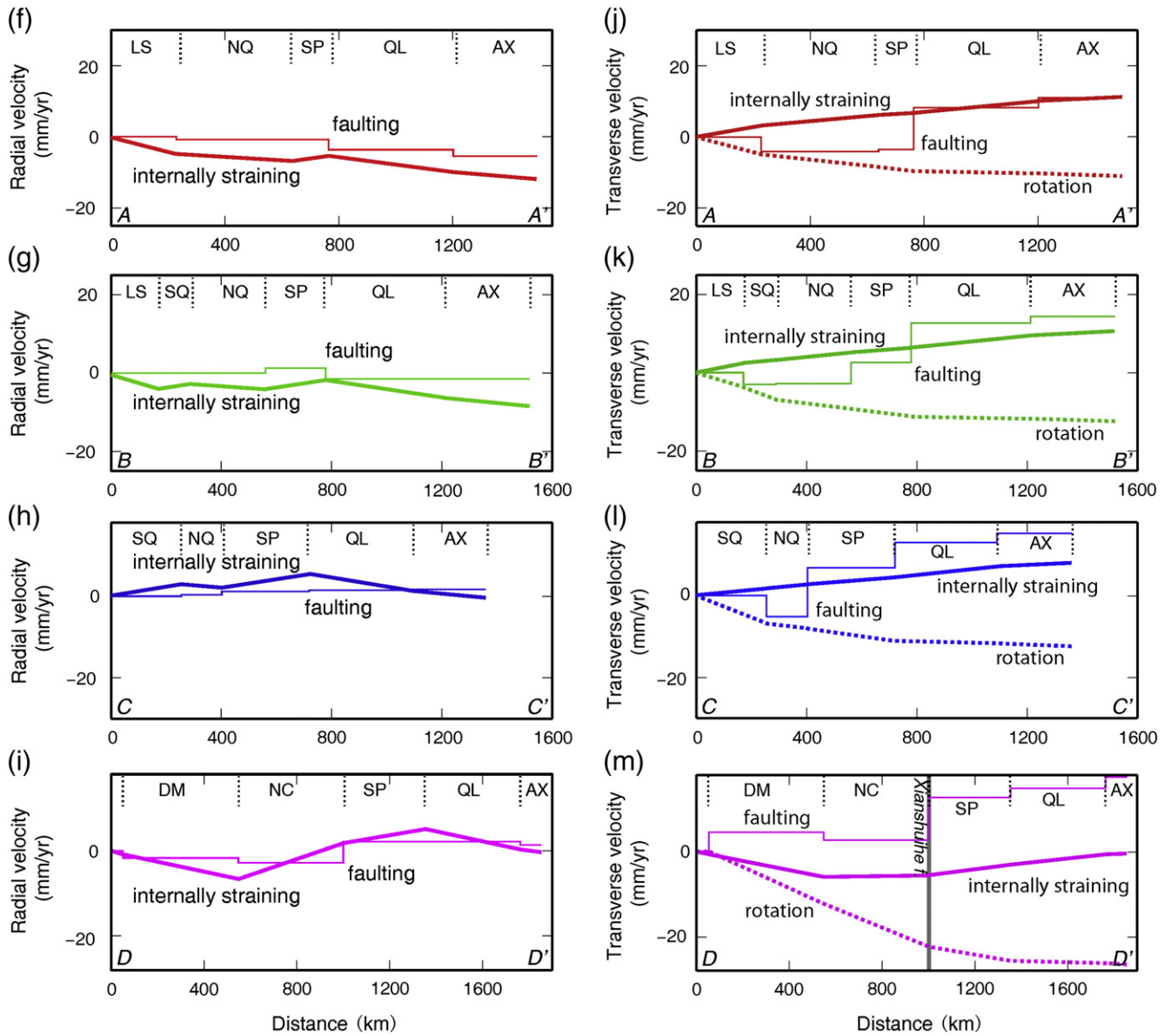


Fig. 8 (continued).

the profile moves southeastward with respect to the southwest end (Fig. 8b–e and j–m), either by clockwise rotation or right-lateral shear. Generally, the velocities predicted by the block model agree with GPS observations in both components (Fig. 8b–e).

In the western part of eastern Tibet, faulting contributes a total of 2 to 5 mm/yr to N–S shortening (AA'; Fig. 8f). The net contribution of faulting decreases to almost zero on BB', CC' and DD' in the east (Fig. 8g, h and i). The internal strain rates of blocks contribute totally 8 to 12 mm/yr shortening in AA' and BB' but decreases to zero on CC' and DD' (Fig. 8f–i). Faulting also contributes 11 to 20 mm/yr eastward motion of eastern Tibet with respect to Eurasia (Fig. 8j–m), while the internal strain rates contribute about 8 to 10 mm/yr ESE extrusion (Fig. 8j–l) except in DD' where it is near zero (Fig. 8m). In contrast to faulting and internal strain, the rotation of the blocks on the plateau contributes about 10 mm/yr WNW movement relative to Eurasian plate (Fig. 8j–l). As shown by DD' (Fig. 8m), the net WNW movement due to spin of blocks amounts to 27 mm/yr in which nearly 20 mm/yr is from the blocks in the area lying south of the Xianshuihe fault that intersects the profile at the distance of 1000 km (Fig. 8m). (Rotation contributes nothing to the radial velocity gradients.)

In terms of N–S shortening of the eastern Tibetan plateau, the internal strain of blocks accounts for major part of surface deformation and is not negligible in comparison with slip rates on major faults. As shown by our results, to balance the total 15 to 20 mm/yr NNE shortening rate, if the contribution from internal strain is ruled out, the faults need an extra 8 to 12 mm/yr shortening, which means the slip rates should be at least two times faster than predicted. With the addition of the extra rates, the prediction of some slip rates, for example, along the Altyn Tagh fault (Fig. 7c) and Jiali fault (Fig. 7f) could approach the geologic results (e.g., Washburn et al., 2003). However, these rapid slip rates turn out to be less supported by newer studies (e.g., Zhang et al., 2007). As to the dip-slip component, it is rarely found on inter-block faults on the eastern Tibetan plateau.

The contribution from internal strain rates of blocks to the ESE extrusion of the eastern Tibetan plateau is about 1.5 times less than that from faulting and is compensated by rotation of blocks; nevertheless, the internal strain is still significant for regional deformation. In southeastern Tibet, as shown by relative velocities on segments ranging from 0 to 1000 km on DD' (Fig. 8m), both internal strain and spin of blocks contribute to the WNW movement relative to Eurasian plate

but the sum of relative velocities due to the strain is less than a fourth of that due to the spin. It appears that the rotation of the surface at the scale of several block dimensions is a first-order mechanism for deformation in southeastern Tibet.

4. Discussion and implications

4.1. Correlation between GPS strain at surface and earthquake deformation

The internal strain rates estimated from the GPS velocity field are estimated at the surface where the deformation can be modified by non-tectonic factors. Therefore, whether the estimated internal strain rates have connections to subsurface deformation requires further analysis. To that end, one method is to compare the strain rates estimated from GPS velocities with those derived from earthquake moment tensors (Kostrov, 1974). However, to obtain reasonable strain rates from earthquakes requires an observation period of earthquakes to be much longer than the recurrence interval of the largest one (Kostrov, 1974), a shorter time results in large uncertainties. An alternative way is to compare the azimuths of principal axes of internal strain rates with those of total earthquake moments since the total moments should have the same eigenvectors as the strain rates.

With the elimination of vertical components of earthquake moments, principal axes in the horizontal plane for each block using 184 Harvard CMT solutions (Fig. 9a) are derived and compared with the principal axes of internal strain rates estimated from GPS data (Fig. 9b–n). Azimuthal distributions of principal axes of individual earthquakes (cyan blue and green sectors) reveal deviations from directions of principal axes of summations of earthquake moments (red and dark blue arrows). In most blocks, the deviations of principal directions for earthquakes are not larger than $\pm 30^\circ$. The small deviations imply that earthquakes within blocks are controlled by the same stress pattern. In the Thailand (TA) and south China (CB) blocks (Fig. 9b and j), deviations are $\pm(30^\circ\text{--}50^\circ)$, showing less consistency in stress patterns. In the blocks having many focal mechanisms (i.e., BM, DM, NQ, QL, SC; Fig. 9c, d, g, i and k), clear consistency is exhibited between the directions of maximum shortening axis of internal strain rates from GPS and those of summations of earthquake moments. It appears that the degree of consistency is not determined by the magnitude of strain rates and is independent of the patterns of principal axes among blocks.

The agreement between GPS- and earthquake-derived strain directions is also seen in blocks SP and AX (Fig. 9h and m); where fewer earthquakes are observed. The discrepancy in the Lhasa block (LS) may be because earthquakes occur along large scale N–S striking

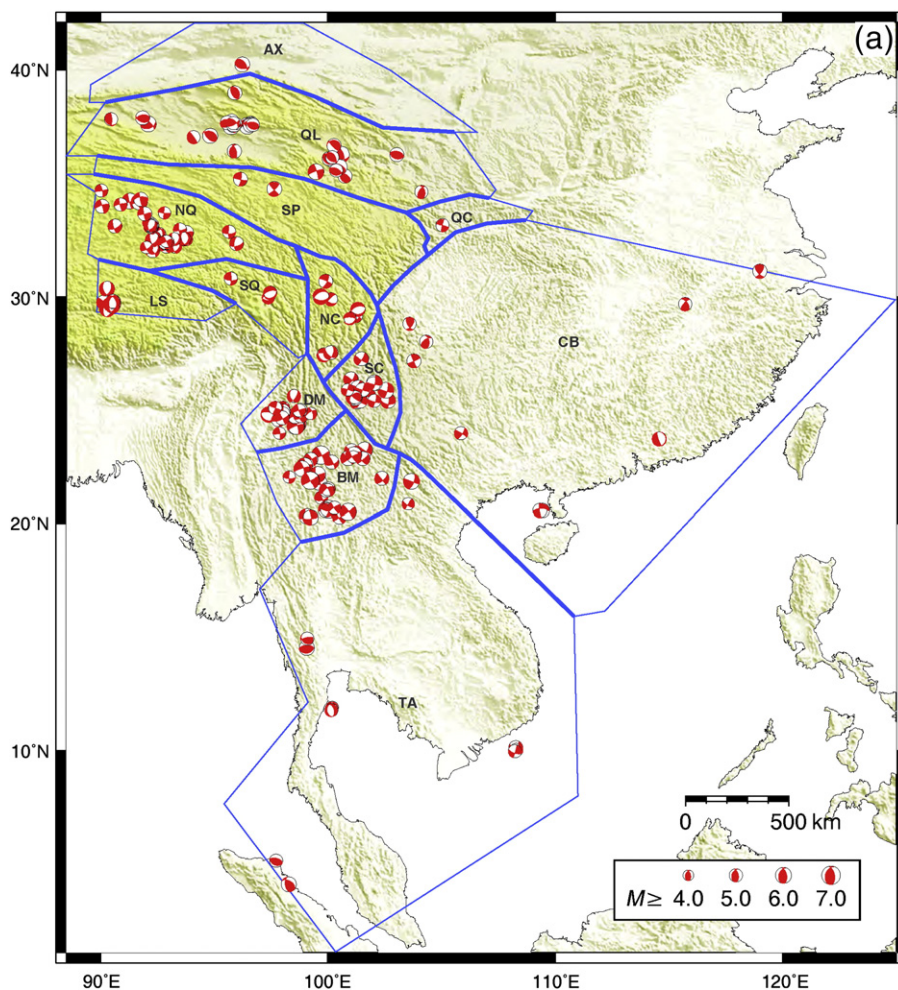


Fig. 9. (a) Focal mechanisms of earthquakes within blocks. The mechanisms are from Harvard CMT solutions (1976–2011, $M \geq 4.0$) and are filtered to exclude events within 50 km of faults (thick blue lines). (b)–(n) Principal axes of earthquakes (Harvard CMT solutions, HCMT) and GPS-derived internal strain rates (GPS) in the horizontal plane are shown with crosses (red for contraction, blue for extension; wedges show uncertainties in magnitude and direction). The length of the arrow is scaled to the maximum component of the average earthquake moments (horizontal components) and the internal strain rate, respectively. Polar histograms (sampled at interval of 10°) show the azimuthal distributions of principal extension (cyan blue) and contraction (green) in horizontal plane of earthquakes. Sectors at the ends of arrows of internal strain rate crosses show uncertainties in azimuths and magnitudes.

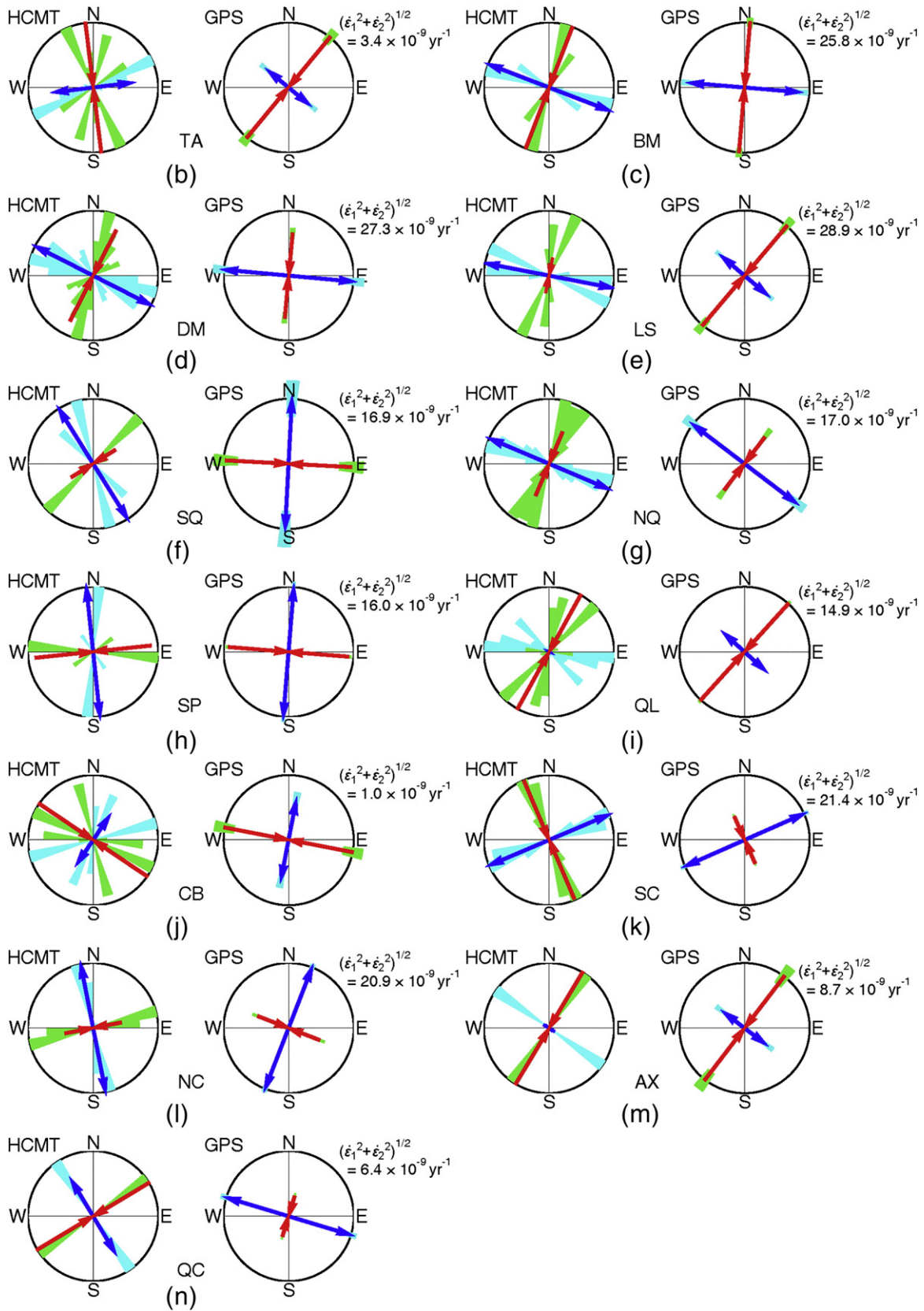


Fig. 9 (continued).

normal faults (e.g., Armijo et al., 1986) which may modify optimum faulting pattern in the near field. The consistency becomes worse ($\sim 50^\circ$) in the Thailand (TA) and Qingchuan (QC) blocks (Fig. 9a and

n), in which the internal GPS-derived strain by itself is not significant. As shown in the above comparison, the internal strain rates in most of the blocks are consistent with earthquake mechanisms suggesting

that the internal strain rates observed at surface also reflect subsurface deformation.

4.2. Effects of scarcity of GPS data and uniform strain assumption

The results of modeling suggest that slip on the West Yushu fault is dextral (Fig. 7b), which is contrary to the geologically observed sinistral slip along the Yushu fault and the adjoining Xianshuihe fault. To test whether the dextral slip is an artifact of the modeling, slip on the west segment of Yushu fault was forced to be sinistral during an inversion, in which case the reduced Chi-square of model increased from 1.588 to 1.602. This small change has a confidence of only 0.55 to be significant and indicates that the few nearby GPS sites cannot constrain the slip sense on the west Yushu fault. By constraining the west Yushu fault to have sinistral slip, the previous prediction of dextral slip on the south boundary fault of the Dian–Burma block is also altered to sinistral slip, which is more consistent with tectonic observations (Xu et al., 2003).

The scarcity of GPS velocities may impact slip rate estimates on other faults. For example, our model predicts a linear, eastward decrease in slip rate along the east Kunlun fault (Fig. 7d), in contrast to the pattern suggested by geological studies that the slip rate is constant through most of its length and drops only near the end (e.g., Kirby et al., 2007). Like the Yushu fault, GPS sites are sparse along middle to west segment of the east Kunlun fault.

Another source of error is that the present block model assumes uniform strain within blocks, which does not account for any spatial variations of rock strength within a block, for example like the rigid Qaidam basin within the Qilian block (QL) (Fig. 10a). Across the Qilian block (Fig. 10b), the gradient of radial velocity (dots) suggests E–W extension in the block as a whole while the transverse gradient (triangles) suggests clockwise rotation for the entire block (Fig. 10b). However, within about 200–300 km of the eastern boundary, the strain rate shows contraction and the rotation rate increases. These variations may be partially explained by elastic strain from nearby faults (Fig. 10b) but still the misfit is significant. The different velocity

pattern in this region could be separated out into another block, but any bounding fault cutting the crust in this area remains unclear. In summary, the prediction of fault slip rates such as that along the middle and west segments of Kunlun fault may be poorly resolved due to data scarcity and the assumption of uniform strain within the blocks model.

5. Conclusions

Both F-tests and the comparison of contributions to relative velocities based on block modeling reveal that the internal strain and spin of blocks are not negligible for describing active deformation of eastern Tibet. About 10 to 20×10^{-9} /yr strain rates are found in most blocks on the plateau, showing that the plateau deforms much faster than the adjacent areas including the south China, Alxa and Thailand blocks where the strain rates are both low magnitude and statistically insignificant. The modeling results show that a deformable block model can also predict strain localization and strike-parallel slip rate variations along major faults on the plateau.

Regarding ESE extrusion of eastern Tibet relative to Eurasian, the internal strain rates in blocks account for a contribution to relative motion at rates of 8 to 12 mm/yr, comparable to the rate of 11 to 15 mm/yr from faulting. On the plateau, the contribution from internal strain of blocks is almost compensated by contrary contribution from vertical axis rotations. From southeast Tibet south to Xianshuihe fault, the contribution from vertical axis rotations becomes the major factor in southeastward extrusion of the southeast Tibet relative to the Eurasian plate. In terms of N–S shortening of the eastern Tibetan plateau, the internal strain rates of blocks contributes a maximum shortening rate of 10 mm/yr across the interior of the plateau west of 95°E . Slip on the major faults contributes over two times less to N–S shortening than internal strain does. The major part of shortening is accommodated by deformation of the Himalayan ranges, amounting to at least 20 mm/yr.

The block kinematics in eastern Tibet exhibit a primary feature that the faulting on a finite number of faults takes up the major part

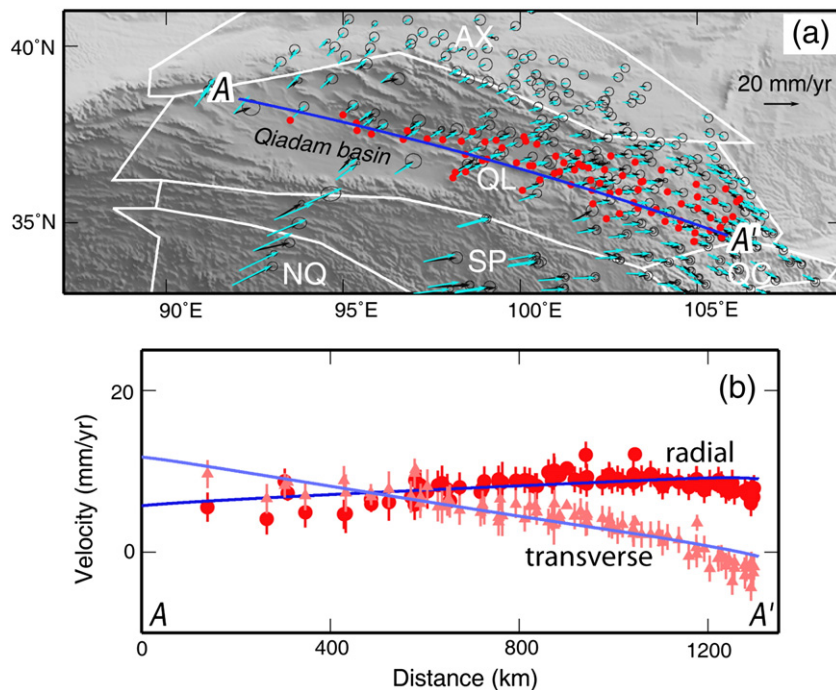


Fig. 10. (a) East–west velocity profile across the Qilian block. Red dots show sites that are projected onto profile. Black vectors are observed with 70% confidence ellipses and green are calculated. (b) Observed GPS components along profile line. Circles show radial component (positive to ESE) and triangles show transverse component (positive to NNE). Blue lines show predicted velocities (dark blue for radial component and light blue for transverse component).

of NW–SE shear while the contraction of blocks takes up major part of N–S compression.

Supplementary data to this article can be found online at <http://dx.doi.org/10.1016/j.tecto.2012.08.006>.

Acknowledgments

We thank Robert W. King for providing combined and rotated GPS velocity fields from multiple sources and for his beneficial discussion on our results. Some work of this study was done during Zhuqi's stay at Rensselaer Polytechnic Institute; he thanks RPI colleagues for their help and suggestions. This study is funded by Special Fund for China Earthquake Research Project (201008003), National Natural Science Foundation of China (40574044) and Joint Visiting Research Project of China Administration of Earthquake and China Scholarship Council.

References

- Armijo, R., Tapponnier, P., Mercier, J.L., Han, T.L., 1986. Quaternary extension in southern Tibet: field observations and tectonic implications. *Journal of Geophysical Research* 91 (B14), 13803–13872.
- Armijo, R., Tapponnier, P., Han, T.L., 1989. Late Cenozoic right-lateral strike-slip faulting in southern Tibet. *Journal of Geophysical Research* 94 (B3), 2787–2838.
- Banerjee, P., Bürgmann, R., Nagarajan, B., Apel, E., 2008. Intraplate deformation of the Indian subcontinent. *Geophysical Research Letters* 35, L18301. <http://dx.doi.org/10.1029/2008GL035468>.
- Bettinelli, P., Avouac, J.-P., Flouzat, M., Jouanne, F., Bollinger, L., Willis, P., Chitrakar, G.R., 2006. Plate motion of India and interseismic strain in the Nepal Himalaya from GPS and DORIS measurements. *Journal of Geodesy* 80, 567–589. <http://dx.doi.org/10.1007/s00190-006-0030-3>.
- Bock, Y., Prawirodirdjo, L., Genrich, J.F., Stevens, C.W., McCaffrey, R., Subarya, C., Puntodewo, S.O., Calais, E., 2003. Crustal motion in Indonesia from Global Positioning System measurements. *Journal of Geophysical Research* 108 (B8), 2367. <http://dx.doi.org/10.1029/2001JB000324>.
- Calais, E., Dong, L., Wang, M., Shen, Z., Vergnolle, M., 2006. Continental deformation in Asia from a combined GPS solution. *Geophysical Research Letters* 33, L24319.
- Chen, G.H., 2006. Structural transformation and strain partitioning along the northeast boundary belt of the Sichuan–Yunnan block [Ph.D. thesis]. Institute of Geology, China Administration of Earthquake.
- Chen, S.F., Wilson, C.J.L., Deng, Q.D., Zhao, X.L., Luo, Z.L., 1994. Active faulting and block movement associated with large earthquakes in the Min Shan and Longmen Mountains, northeastern Tibetan Plateau. *Journal of Geophysical Research* 99 (B12), 24025–24038.
- Chen, Z., Burchfiel, B.C., Liu, Y., King, R.W., Royden, L.H., Tang, W., Wang, E., Zhao, J., Zhang, X., 2000. Global positioning system measurements from eastern Tibet and their implications for India/Eurasia intercontinental deformation. *Journal of Geophysical Research* 105 (B7), 16215–16227.
- Chen, Q.Z., Freymueller, J.T., Wang, Q., Yang, Z.Q., Xu, C.J., Liu, J.N., 2004. A deforming block model for the present-day tectonic of Tibet. *Journal of Geophysical Research* 109, B01403. <http://dx.doi.org/10.1029/2002JB002151>.
- Chung, L., Chen, Y., Lai, K., Yin, G., Cao, Z., 2007. Is Jiali fault still an active fault in the late Pleistocene? American Geophysical Union, Fall Meeting 2007, abstract #T31D-0676.
- Deng, Q.D., 2007. China active tectonic map. Seismological Press, scale 1:4 000 000, 1 sheet.
- England, P., Molnar, P., 2005. Late Quaternary to decadal velocity fields in Asia. *Journal of Geophysical Research* 110, B12401. <http://dx.doi.org/10.1029/2004JB003541>.
- Gan, W.J., Zhang, P.Z., Shen, Z.K., Niu, Z.J., Wang, M., Wan, Y.G., Zhou, D.M., Cheng, J., 2007. Present-day crustal motion within the Tibetan Plateau inferred from GPS measurements. *Journal of Geophysical Research* 112, B08416. <http://dx.doi.org/10.1029/2005JB004120>.
- Gaudemer, Y., Tapponnier, P., Meyer, B., Peltzer, G., Guo, S.M., Chen, Z.T., Dai, H.G., Cifuentes, I., 1995. Partitioning of crustal slip between linked, active faults in the eastern Qilian Shan, and evidence for a major seismic gap, the 'Tianzhu gap', on the western Haiyuan fault, Gansu (China). *Geophysical Journal International* 120, 599–645.
- Guo, S.M., Ji, F.J., et al., 2001. The Honghe Active Fault Zone. Ocean Press, Beijing.
- Guo, J.M., Lin, A., Sun, G.Q., Zheng, J.J., 2007. Surface ruptures associated with the 1937 M 7.5 Tuosuo lake and the 19763 M 7.0 Alake earthquakes and the paleoseismicity along the Tuosuo lake segment of the Kunlun fault, Northern Tibet. *Bulletin of the Seismological Society of America* 97 (2), 474–496.
- He, H.L., Ikeda, Y., Song, F.M., Dong, X.Q., 2002. Late Quaternary slip rate of the Xiaojiang fault and its implication. *Seismology and Geology* 24 (1), 14–26.
- Jade, S., Mukul, M., Bhattacharyya, A.K., Vijayan, M.S.M., Jaganathan, S., Kumar, A., Tiwari, R.P., Kumar, A., Kalita, S., Sahu, S.C., Krishna, A.P., Gupta, S.S., Murthy, M.V.R.L., Gaur, V.K., 2007. Estimates of interseismic deformation in Northeast India from GPS measurements. *Earth and Planetary Science Letters* 263, 221–234.
- King, R.W., Shen, F., Burchfiel, B.C., Royden, L.H., Wang, E., Chen, Z.L., Liu, Y.P., Zhang, X.Y., Zhao, J.X., Li, Y.L., 1997. Geodetic measurement of crustal motion in southwest China. *Geology* 25, 179–182.
- Kirby, E., Harkins, N., Wang, E., Shi, X.H., Fan, C., Burbank, D., 2007. Slip rate gradients along the eastern Kunlun fault. *Tectonics* 26, TC2010. <http://dx.doi.org/10.1029/2006TC002033>.
- Kostrov, B.V., 1974. Seismic moment and energy of earthquakes, and seismic flow of rock. *Izvestiya Academy Science, USSR. Physics of Solid Earth* 1, 23–44.
- Lasserre, C., Gaudemer, Y., Tapponnier, P., Meriaux, A.-S., Van der Woerd, J., Yuan, D.Y., Ryerson, F.J., Finkel, R.C., Caffee, M.W., 2002. Fast late Pleistocene slip rate on the Leng Long Ling segment of the Haiyuan fault, Qinghai, China. *Journal of Geophysical Research* 107 (B11), 2276. <http://dx.doi.org/10.1029/2000JB000060>.
- Li, H.B., Van der Woerd, J., Tapponnier, P., Klinger, Y., Qi, X.X., Yang, J.S., Zhu, Y.T., 2005. Slip rate on the Kunlun fault at Hongshui Gou, and recurrence time of great events comparable to the 14/11/2001, Mw 7.9 Kokoxili earthquake. *Earth and Planetary Science Letters* 237, 285–299.
- Li, C.Y., Zhang, P.-Z., Yin, J.H., Min, W., 2009. Late Quaternary left-lateral slip rate of the Haiyuan fault, northeastern margin of the Tibetan Plateau. *Tectonics* 28, TC5010. <http://dx.doi.org/10.1029/2008TC002302>.
- Lin, A.M., Guo, J.M., 2008. Nonuniform slip rate and millennial recurrence interval of large earthquakes along the eastern segment of the Kunlun fault, Northern Tibet. *Bulletin of the Seismological Society of America* 98 (6), 2866–2878.
- Lin, A.M., Guo, J.M., Kano, K.-I., Awata, Y., 2006. Average slip rate and recurrence interval of large-magnitude earthquakes on the western segment of the strike-slip Kunlun fault, Northern Tibet. *Bulletin of the Seismological Society of America* 96 (5), 1597–1611.
- Loveless, J.P., Meade, B.J., 2011. Partitioning of localized and diffuse deformation in the Tibetan Plateau from joint inversion of geologic and geodetic observation. *Earth and Planetary Science Letters* 303, 11–24.
- McCaffrey, R., 1996. Slip partitioning at convergent plate boundaries of SE Asia. *Geological Society, London, Special Publications* 106, 3–18.
- McCaffrey, R., 2005. Block kinematics of the Pacific–North America plate boundary in the southwestern United States from inversion of GPS, seismological, and geologic data. *Journal of Geophysical Research* 110, B07401. <http://dx.doi.org/10.1029/2004JB003307>.
- McCaffrey, R., Oamar, A.L., King, R.W., Wells, R., Khazaradze, G., Williams, C.A., Stevens, C.W., Vollick, J.J., Zwick, P.C., 2007. Fault locking, block rotation and crustal deformation in the Pacific Northwest. *Geophysical Journal International* 169, 1315–1340.
- Meade, B.J., 2007. Present-day kinematics at the India–Asia collision zone. *Geology* 35 (1), 81–84. <http://dx.doi.org/10.1130/G22924A>.
- Meade, B.J., Hager, B.H., 2005. Block models of crustal motion in southern California constrained by GPS measurements. *Journal of Geophysical Research* 110, B03403.
- Molnar, P., Dayem, K.E., 2010. Major intracontinental strike-slip faults and contrasts in lithospheric strength. *Geosphere* 6 (4), 444–467.
- Molnar, P., Lyon-Caen, H., 1989. Fault plane solutions of earthquakes and active tectonics of the Tibetan Plateau and its margins. *Geophysical Journal International* 99, 123–153.
- Pan, G.T., and Ding, J., 2004. The geological map of Qinghai–Xizhang (Tibet) and adjacent areas. Chengdu Institute of Geology and Mineral Resources, China Geological Survey, Chengdu Cartographic Publishing House, scale 1:500000, 1 sheet.
- Press, W.H., Teukolsky, S.A., Vetterling, W.T., Flannery, B.P., 1992. *Numerical Recipes in Fortran 77, the Art of Scientific Computing*, Second ed. Press Syndicate of the University of Cambridge, New York.
- Shen, Z.K., Lü, J.N., Wang, M., Bürgmann, R., 2005. Contemporary crustal deformation around the southeast borderland of the Tibetan Plateau. *Journal of Geophysical Research* 110, B11409.
- Simons, W.J.F., Socquet, A., Vigny, C., Ambrosius, A.C., Abu, S.H., Promthong, C., Subarya, C., Sarsito, D.A., Matheussen, S., Morgan, P., Spakman, W., 2007. A decade of GPS in Southeast Asia: resolving Sundaland motion and boundaries. *Journal of Geophysical Research* 112, B06420. <http://dx.doi.org/10.1029/2005JB003868>.
- Socquet, A., Vigny, C., Chamot-Rooke, N., Simons, W., Rangin, C., Ambrosius, B., 2006. India and Sunda plates motion and deformation along their boundary in Myanmar determined by GPS. *Journal of Geophysical Research* 111, B05406. <http://dx.doi.org/10.1029/2005JB003877>.
- Sol, S., Meltzer, A., Bürgmann, R., van der Hilst, R.D., King, R., Chen, Z., Koons, P.O., Lev, E., Liu, Y.P., Zeitler, P.K., Zhang, X., Zhang, J., Zurek, B., 2007. Geodynamics of the southeastern Tibetan Plateau from seismic anisotropy and geodesy. *Geology* 35 (6), 563–566. <http://dx.doi.org/10.1130/G23408A.1>.
- Song, F.M., Wang, Y.P., Yu, W.X., Cao, Z.Q., Shen, X.H., Shen, J., 1998. Xiaojiang Fault Zone. Seismological Press, Beijing.
- Stein, S., Gordon, R.G., 1984. Statistical tests of additional plate boundaries from plate motion inversions. *Earth and Planetary Science Letters* 69, 401–412.
- Tapponnier, P., Xu, Z.Q., Roger, F., Meyer, B., Arnaud, N., Wittlinger, G., Yang, J.S., 2001. Oblique stepwise rise and growth of the Tibet Plateau. *Science* 294, 1671–1677.
- Thatcher, W., 2007. Microplate model for the present-day deformation of Tibet. *Journal of Geophysical Research* 112, B01401. <http://dx.doi.org/10.1029/2005JB004244>.
- Thatcher, W., 2009. How the continents deform: the evidence from tectonic geodesy. *Annual Review of Earth and Planetary Sciences* 37, 14.1–14.26. <http://dx.doi.org/10.1146/annurev.earth.031208.100035>.
- Van der Woerd, J., Ryerson, F.J., Tapponnier, P., Meriaux, A.-S., Gaudemer, Y., Meyer, B., Finkel, R.C., Caffee, M.W., Zhao, G.G., Xu, Z.Q., 2000. Uniform slip-rate along the Kunlun fault: implications for seismic behaviour and large-scale tectonics. *Geophysical Research Letters* 27 (16), 2353–2356.
- Van der Woerd, J., Ryerson, F.J., Tapponnier, P., Meriaux, A.-S., Meyer, B., Gaudemer, Y., Finkel, R.C., Caffee, M.W., Zhao, G.G., Xu, Z.Q., 2002. Uniform postglacial slip-rate along the central 600 km of the Kunlun fault (Tibet), from ²⁶Al, ¹⁰Be, and ¹⁴C dating of riser offsets, and climatic origin of the regional morphology. *Geophysical Journal International* 148, 356–388.
- Washburn, Z., Arrowsmith, J.R., Dupont-Nivet, G., Wang, X.F., Zhang, Y.Q., Chen, Z.D., 2003. Paleoseismology of the Xorxol segment of the central Altyn Tagh fault, Xinjiang, China. *Annals of Geophysics* 46 (5), 1015–1034.

- Wen, X., Xu, X., Zheng, R., Xie, Y., Wan, C., 2003. Average slip-rate and recent large earthquake ruptures along the Garzê–Yushu fault. *Science in China Series D: Earth Sciences* 46 (Suppl. 2), 276–288. <http://dx.doi.org/10.1360/03dz0022>.
- Xu, X.W., Wen, X.Z., Zheng, R.Z., Ma, W.T., Song, F.M., Yu, G.H., 2003. Pattern of latest tectonic motion and its dynamics for active blocks in Sichuan–Yunnan region, China. *Science in China Series D: Earth Sciences* 46 (Suppl. 2), 210–226. <http://dx.doi.org/10.1360/03dz0017>.
- Xu, X.W., Zhang, P.Z., Wen, X.Z., Qin, Z.L., Chen, G.H., Zhu, A.L., 2005. Features of active tectonics and recurrence behaviors of strong earthquakes in the western Sichuan province and its adjacent regions. *Seismology and Geology* 27 (3), 446–461.
- Zhang, P.Z., Burchfiel, B.C., Molnar, P., Zhang, W.Q., Jiao, D.C., Deng, Q.D., Wang, Y.P., Leigh, R., Song, F.M., 1991. Amount and style of late Cenozoic deformation in the Liupan Shan area, Ningxia autonomous region, China. *Tectonics* 10 (6), 1111–1129.
- Zhang, P.Z., Shen, Z.K., Wang, M., Gan, W.J., Bürgmann, R., Molnar, P., Wang, Q., Niu, Z.J., Sun, J.Z., Wu, J.C., Sun, H.R., You, X.Z., 2004. Continuous deformation of the Tibetan Plateau from Global Positioning System data. *Geology* 32, 809–812. <http://dx.doi.org/10.1130/G20554.1>.
- Zhang, P.Z., Molnar, P., Xu, X.W., 2007. Late Quaternary and present-day rates of slip along the Altyn Tagh fault, northern margin of the Tibetan Plateau. *Tectonics* 26, TC5010. <http://dx.doi.org/10.1029/2006TC002014>.
- Zhang, Z.Q., Zhang, P.-Z., Wang, Q.L., 2010. The structure and seismogenic mechanism of Longmenshan high dip-angle reverse fault. *Chinese Journal of Geophysics* 53 (9), 2068–2082.
- Zheng, Y., Ma, H.S., Lü, J., Ni, S.D., Li, Y.C., Wei, S.J., 2009. Source mechanism of strong aftershocks ($M_s \geq 5.6$) of the 2008/05/12 Wenchuan earthquake and the implication for seismotectonics. *Science in China Series D: Earth Sciences* 52 (6), 739–753. <http://dx.doi.org/10.1007/s11430-009-0074-3>.
- Zhou, R.J., Li, Y., Densmore, A., Ellis, M.A., He, Y.L., Wang, F.L., Li, X.G., 2006. Active tectonics of the eastern margin of the Tibet Plateau. *Journal of Mineral Petrology* 26 (2), 40–51.